Comparative Biochemistry and Physiology - Part D: Genomics and Proteomics 59 (2026) 101787

Contents lists available at ScienceDirect

Comparative Biochemistry and Physiology - Part D: Genomics and Proteomics

journal homepage: www.elsevier.com/locate/cbpd

Research article

Dual-layered epigenetic regulation links water body size constraints to somatic growth in an allotetraploid fish

Yiyan Zeng [a,1], Jinhui Zhang [a,1], Qingxi Wang [d,1], Xiaohuan Han [a], Ling Liu [a], Kai Yang [a], Ruyi Zhang [a], Kaikun Luo [a], Li Ren [a,b,c,*], Shaojun Liu [a,b,c,*]

[a] Engineering Research Center of Polyploid Fish Reproduction and Breeding of the State Education Ministry, College of Life Sciences, Hunan Normal University, Changsha, 410081, Hunan, China
[b] Yuelushan Laboratory, Changsha, 410081, Hunan, China
[c] Hunan Yuelu Mountain Science and Technology Co., Ltd. for Aquatic Breeding, Changsha, 410081, Hunan, China
[d] Hunan Traditional Chinese Medical College, Changsha, 410081, Hunan, China

ARTICLE INFO

Edited by Chris Martyniuk

Keywords:
Subgenome
Chromatin accessibility
Environmental adaptation
Body size divergence
Allotetraploid fish

ABSTRACT

Polyploidy endows fish with genomic plasticity to colonize restricted environments, yet the molecular mechanisms linking ecological constraints to somatic growth remain elusive. Here, we investigated the adaptive response of an allotetraploid lineage (*Carassius auratus* × *Cyprinus carpio*) to contrasting water body sizes using multi-omics approaches. We found that spatial constraints triggered targeted transcriptional remodeling specifically in the eye and muscle. This response effectively links sensory perception to growth regulation. Meanwhile, we identified a dual-layered epigenetic strategy. Environmental stress forced a reduction in the active gene pool via promoter silencing, while concurrently depressing the expression levels of growth-related structural genes through enhancer inhibition. Interestingly, this plasticity exhibited striking subgenome asymmetry. The *Cyprinus* subgenome displayed higher epigenetic responsiveness and acted as the primary adaptive buffer, exemplified by the targeted repression of a *Cyprinus*-derived enhancer regulating the mTOR gene *rps6kb1a*. Our findings demonstrate how subgenome-biased epigenetic remodeling aligns growth phenotypes with ecological constraints, offering molecular insights into the evolutionary success of polyploids in fragmented habitats.

1. Introduction

Polyploidization (whole-genome duplication) and hybridization are recognized as primary driving forces in fish evolution, endowing species with genomic redundancy that fuels adaptive diversification and niche expansion (Van de Peer et al., 2017, 2021). Large-scale biogeographical and phylogeographic analyses have recently demonstrated that polyploid fishes exhibit substantial adaptive potential, allowing them to colonize broader ecological niches and persist in more extreme or fluctuating environments—such as high latitudes and high-altitude plateaus—compared to their diploid relatives (Liu et al., 2017; Li and Guo, 2020; David, 2022). Within the diverse Cyprinidae family, the goldfish (*Carassius auratus*) and the common carp (*Cyprinus carpio*) belong to the subfamily Cyprininae, a lineage that itself originated from an ancient allopolyploidization event approximately 13.75 million years ago (Mya) (Xu et al., 2014, 2019; Chen et al., 2020; Luo et al., 2020). Beyond this ancient duplication, the nascent allotetraploid lineage derived from their recent hybridization harbors two distinct ancestral subgenomes, creating a unique genomic architecture. In such hybrid genomes, homoeologous gene pairs often exhibit biased expression or asymmetric epigenetic regulation (Liu et al., 2016; Ren et al., 2022). This genomic asymmetry is hypothesized to provide a reservoir of plasticity: one subgenome may maintain fundamental functions while the other is released from constraint to evolve novel responses to environmental fluctuations. Consequently, the allotetraploid hybrid lineage of goldfish and common carp thus presents an ideal model for investigating the coordination of phenotypic plasticity, particularly growth traits, by subgenome interplay under divergent environmental pressures.

Environmental constraints, particularly water body size, profoundly influence the life history and morphology of freshwater fish (Woolnough

* Corresponding authors at: Engineering Research Center of Polyploid Fish Reproduction and Breeding of the State Education Ministry, College of Life Sciences, Hunan Normal University, Changsha, 410081, Hunan, China.
E-mail addresses: rl@hunnu.edu.cn (L. Ren), lsj@hunnu.edu.cn (S. Liu).
[1] These authors contributed equally to this work.

https://doi.org/10.1016/j.cbd.2026.101787
Received 29 December 2025; Received in revised form 15 February 2026; Accepted 23 February 2026
Available online 3 March 2026
1744-117X/© 2026 Elsevier Inc. All rights are reserved, including those for text and data mining, AI training, and similar technologies.

et al., 2009). Unlike mammals, fish possess the unique characteristic of indeterminate growth, allowing them to adjust their body size continuously in response to spatial constraints and resource availability—a phenomenon known as the "spatial effect" (Parsons and Robinson, 2006; Ahti et al., 2020; Audzijonyte et al., 2020; Oke et al., 2020). This plasticity is largely driven by the dynamic remodeling of skeletal muscle, the primary tissue determining somatic growth. While phenotypic responses to water body size are well-documented, the underlying molecular mechanisms remain elusive. How do external spatial cues translate into chromatin remodeling and transcriptional changes within muscle tissue? Recent advances suggest that chromatin accessibility (ATAC-seq) and histone modifications (e.g., H3K27ac) act as the interface between the environment and the genome, controlling gene expression through the distinct logic of promoters (which often act as on/off switches) and enhancers (which fine-tune expression levels) (Thorson et al., 2017; Abdelnour et al., 2024).

Although genomic plasticity in nascent allopolyploids has been characterized regarding copy number variations and expression bias, the epigenetic regulatory logic driving environmental adaptation remains poorly understood. Specifically, it is unclear how distinct water body sizes reshape the epigenomic landscape of key growth-related tissues and whether different subgenomes contribute asymmetrically to this regulation. To address this, we reared the F_2 generation of allotetraploid hybrids under contrasting small and large water environments. We first performed a multi-tissue transcriptomic screen to identify the tissues most sensitive to environmental constraints, pinpointing the muscle and eye as hotspots of transcriptional divergence. Subsequently, we constructed a high-resolution map of chromatin accessibility and H3K27ac modifications in muscle tissue. Through integrated multi-omics analyses, we aim to elucidate: (1) the distinct roles of promoter accessibility versus enhancer activity in modulating growth-related gene networks; and (2) the differential contribution of the two ancestral subgenomes to epigenetic plasticity. Our findings provide novel insights into how allopolyploid fish utilize complex regulatory strategies—involving enhancer modulation and subgenome-specific responses—to adapt their body size to spatial environmental constraints.

2. Results

2.1. Remodeling of transcriptional landscapes across tissues and subgenomes

To investigate the impact of water body size on gene expression over multi-generational domestication, F_2 generation allotetraploid hybrids (*Carassius auratus* × *Cyprinus carpio*) were reared in contrasting small and large water environments, with other variables (pH, light, temperature, feeding) kept constant. Individuals in the large water environments ($4nR_2C_2$-B) exhibited significantly greater growth compared to those in the small water environments ($4nR_2C_2$-S). Specifically, the $4nR_2C_2$-B group showed significantly higher body weight, body length, and body height compared to the $4nR_2C_2$-S ($p < 0.05$), with no significant sex differences in these traits ($p > 0.05$) (Fig. 1A). We performed RNA-seq on 11 tissues from representative individuals and quantified expression using the combined reference genome of the diploid progenitors.

Clustering analysis revealed that the intestine, ovary, eye, and muscle exhibited the most significant transcriptomic divergence between the two environmental populations (median divergence >0.32) (Figs. 1B, S1). Furthermore, in addition to muscle (20.73%), eye (25.14%), and intestine (33.43%), the testis (35.26%) and liver (30.67%) displayed high transcriptomic plasticity, as evidenced by the proportion of differentially expressed genes (DEGs) (Fig. S2). Given the critical roles of the eye and muscle in environmental perception and somatic growth, respectively, these results suggest that water body size primarily drives adaptive phenotypic changes by reshaping the expression profiles of these tissues.

Principal Component Analysis (PCA) highlighted distinct intra-population patterns, greater dispersion of points within a group indicates higher inter-individual expression heterogeneity, whereas tighter clustering indicates lower heterogeneity. Individuals in the small water environment showed reduced expression heterogeneity in the eye, muscle, and pituitary compared to those in the large water environment (Figs. 1C, S3). This transcriptional convergence suggests that the small water environment imposes stronger regulatory constraints on these tissues. At the subgenome level, we observed a striking asymmetry: in tissues such as the brain, heart, kidney, and spleen, the subgenome C (originating from goldfish) exhibited significantly higher expression heterogeneity among individuals than the subgenome R (originating from common carp) (Fig. 1C). This implies that the subgenome R is subject to stricter regulation, whereas the subgenome C may offer greater plasticity in response to environmental fluctuations.

Further analysis of DEGs in the highly plastic muscle and eye tissues revealed extensive expression changes (Muscle: 8348 DEGs; Eye: 15,819 DEGs) (Fig. 1D). GO enrichment analysis showed that these DEGs were significantly enriched in biological processes related to growth, such as muscle structure development (GO: 0061061) and skeletal muscle organ development (GO: 0060538) (Fig. 1E), linking environmental stress directly to phenotypic modulation via structural gene regulation.

2.2. Global epigenetic landscape and subgenome asymmetry in muscle

To decipher the epigenetic mechanisms underlying environmentally induced growth plasticity, we performed ATAC-seq and H3K27ac CUT&Tag on muscle tissue. PCA revealed that the samples were clearly clustered by group. Furthermore, Pearson correlation analysis demonstrated high reproducibility among biological replicates (Fig. S4). Quality control confirmed that open chromatin regions (ATAC peaks) and H3K27ac signals were enriched in intergenic regions, introns, and near transcription start sites (TSS) (Fig. S5), showing a positive correlation with gene expression (Figs. S6, 2A).

The water environment significantly reshaped the chromatin landscape. In terms of chromatin accessibility, the small water population ($4nR_2C_2$-S) exhibited a more open landscape (508,622 peaks) compared to the large water population ($4nR_2C_2$-B, 411,694 peaks). Conversely, for H3K27ac modification, the trend was reversed: $4nR_2C_2$-S displayed significantly fewer active histone peaks (54,147) than $4nR_2C_2$-B (75,481). This pattern of "increased accessibility but decreased active modification" suggests that the small water environment may induce a widespread poised chromatin state or non-functional openness. Importantly, epigenetic markers showed a biased distribution between subgenomes. Regardless of the environment, the subgenome C consistently displayed a higher density of ATAC-seq and H3K27ac peaks compared to the subgenome R (Fig. 2B, C). This aligns with the higher transcriptomic plasticity of the subgenome C, suggesting it plays a more dynamic role in the epigenetic adaptation of the allotetraploid.

2.3. Identification and functional characterization of enhancers

To investigate the role of distal regulation, we integrated ATAC-seq and H3K27ac data to identify 16,271 putative enhancers. Of these, 4206 were shared between populations, while 8571 and 3494 were specific to the large and small water populations, respectively (Fig. 3A). These regions were predominantly located in distal intergenic and intronic regions, consistent with canonical enhancer features (Fig. 3B).

Differential analysis identified 333 enhancers with significant changes in accessibility and 2605 with changes in H3K27ac modification (Fig. 3C). Functional enrichment of their target genes revealed that these environmentally responsive enhancers regulate key growth processes, including myofibril assembly (GO: 0030239), muscle structure development (GO: 0061061), muscle cell development (GO: 0055001), and the mTOR signaling pathway (map04150) (Figs. 3D, S7). These findings strongly suggest that epigenetic remodeling at the enhancer

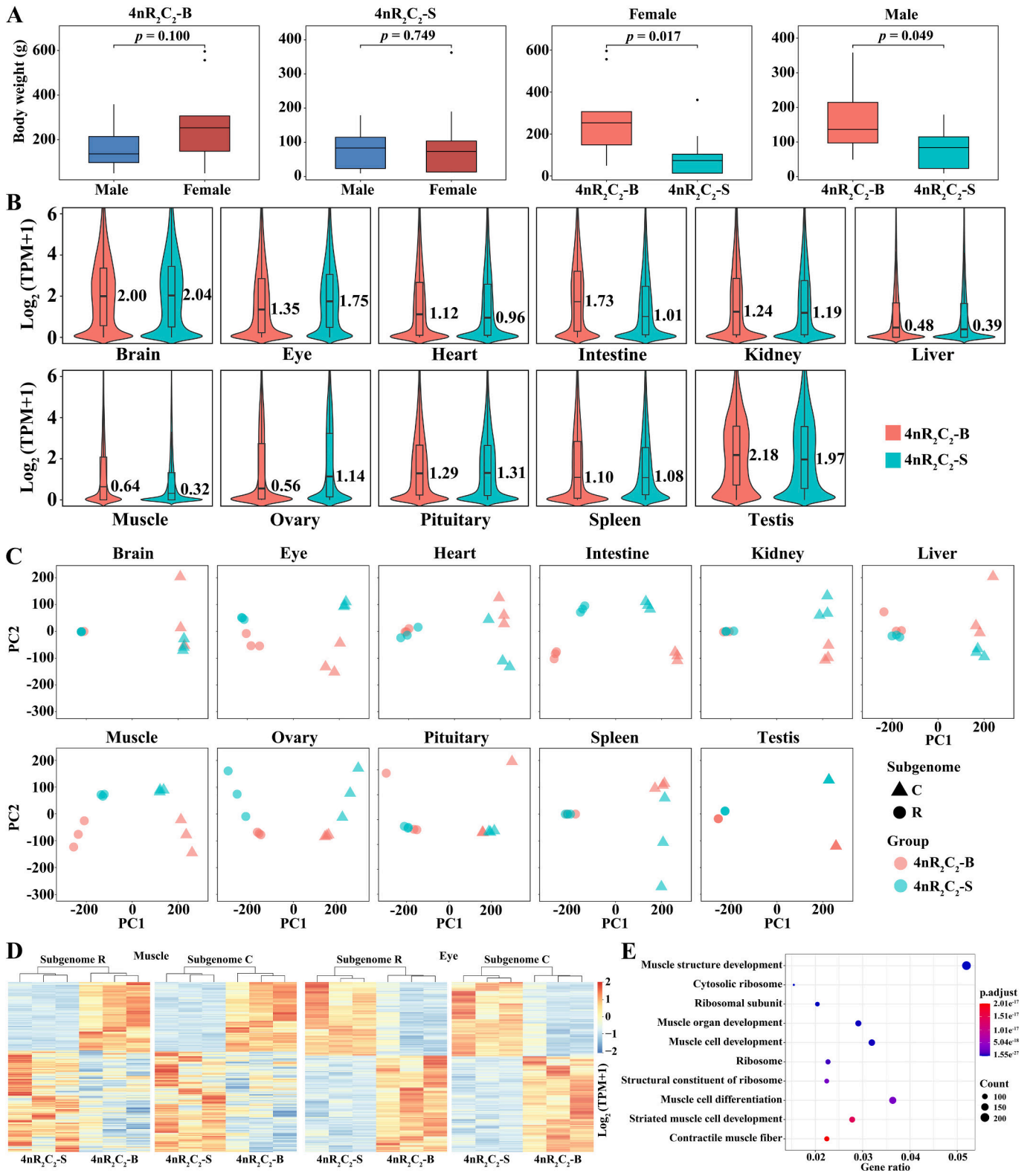


Fig. 1. Phenotypic differences, transcriptomic landscape and tissue-specific remodeling in the allotetraploid hybrid under contrasting water environments. (A) Body weight comparisons between sexes within each group ($4nR_2C_2$-B and $4nR_2C_2$-S) and between groups within each sex. (B) Principal component analysis (PCA) of gene expression profiles across 11 tissues based on total expression of homoeologous gene pairs, highlighting tissue specificity and environmental clustering. (C) Comparison of the median divergence in gene expression between the two water environments across different tissues. The x-axis represents tissues, and the y-axis indicates the median value of expression differences, highlighting high plasticity in muscle and eye. (D) Hierarchical clustering heatmap of differentially expressed genes (DEGs) in muscle and eye tissues. The color scale represents row-scaled expression values (*Z*-scores). (E) Gene Ontology (GO) functional enrichment analysis of DEGs identified in muscle tissue. Dot size indicates the number of genes, and color intensity represents statistical significance.

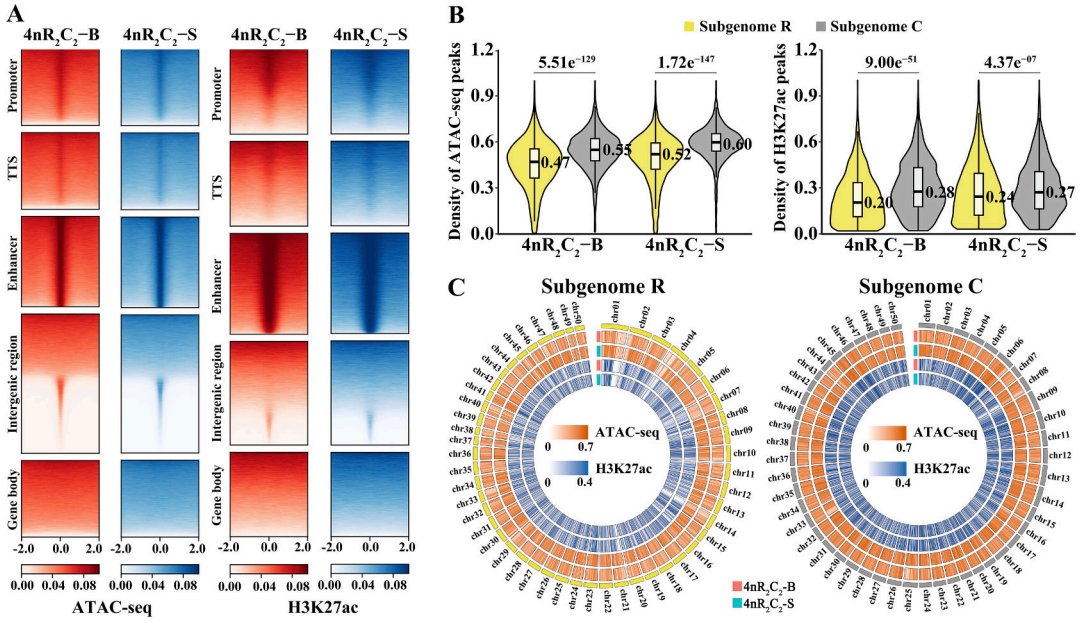


Fig. 2. Epigenomic landscapes of chromatin accessibility and H3K27ac modification in muscle tissue. (A) Metagene profiles illustrating the average aggregation of chromatin accessibility (ATAC-seq) and histone acetylation (H3K27ac) across key genomic features, including transcription start sites (TSS), enhancer regions, and gene bodies. (B) Density distribution of ATAC-seq and H3K27ac peaks across the subgenomes R and C in $4nR_2C_2$-B and $4nR_2C_2$-S populations. Statistical significance was determined using Student's *t*-test. (C) Chromosomal distribution of ATAC-seq and H3K27ac peaks across the subgenomes R and C in both populations, highlighting the asymmetric epigenetic landscape between subgenomes.

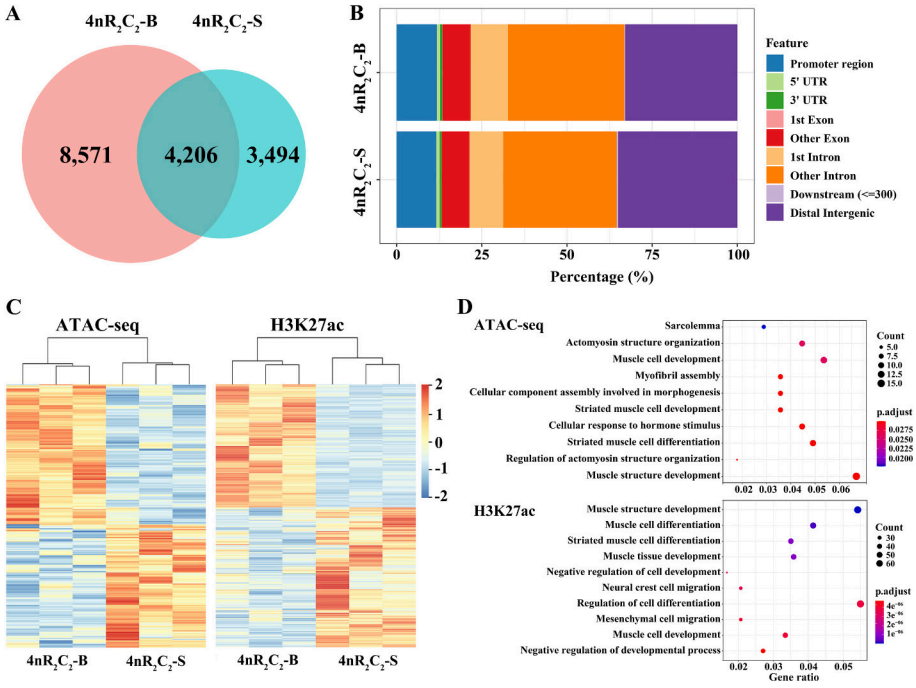


Fig. 3. Identification, characterization, and functional implication of environmentally responsive enhancers. (A) Venn diagram displaying the number of shared and population-specific putative enhancers identified in the $4nR_2C_2$-B and $4nR_2C_2$-S populations. (B) Genomic annotation of identified enhancers showing their distribution across functional elements, including promoters, introns, and distal intergenic regions. (C) Heatmaps of normalized ATAC-seq and H3K27ac signal intensities at identified differential enhancer regions. Each row represents a genomic region, and color intensity indicates signal coverage. (D) Gene Ontology (GO) enrichment analysis of target genes associated with enhancers showing significant differences in chromatin accessibility (top) or H3K27ac modification (bottom). Key terms related to muscle development are highlighted.

level is a driver of population differentiation in muscle development.

2.4. Differential regulatory mechanisms of promoters and enhancers

To elucidate the regulatory mechanism of different genomic elements in environmental adaptation, we first statistically characterized

the global changes in chromatin states. Differential analysis of ATAC-seq identified 11,201 differentially accessible regions (DARs) between the two populations, showing a balanced distribution of increased (5761) and decreased (5440) accessibility in the small water population (Fig. 4A). Similarly, analysis of H3K27ac CUT&Tag data revealed 6997 differentially modified peaks (DPs), which also exhibited a bidirectional trend of gains and losses (Fig. 4A). These results indicate that the allotetraploid hybrid undergoes extensive and dynamic epigenetic remodeling in response to water body size constraints.

However, mapping these differential sites to genomic functional elements revealed a distinct regulatory preference. The proportion of DARs (1.43%) and DPs (5.79%) located in promoter regions was significantly higher than that in enhancer regions (0.53% and 3.21%, respectively), and Chi-square tests confirmed that promoters were significantly more sensitive to epigenetic remodeling than enhancers ($p < 0.001$, Fig. 4B). Specifically, promoters in the small water environment predominantly exhibited a coordinated loss of both chromatin accessibility and H3K27ac signals (Tables S9–S10). This epigenetic silencing aligns perfectly with the transcriptomic observation that the total number of expressed genes was significantly reduced in the small water population compared to the large water population (39,256 vs. 47,553). These findings strongly suggest that environmental stress tends to "switch off" promoter states to block transcription initiation, thereby determining the binary status of gene expression.

In contrast, although enhancers showed a lower proportion of differential sites, they also displayed a clear trend of signal attenuation in the small water population (Tables S9–S10). Unlike the "on/off" mechanism observed at promoters, the reduction in enhancer activity paralleled the decrease in median gene expression levels observed in the small water population (0.32 vs. 0.64). This implies that enhancers function primarily as "rheostats" during environmental adaptation, fine-tuning transcriptional abundance through quantitative changes in epigenetic modification strength rather than determining gene presence or absence.

In contrast, some non-promoter and non-enhancer regions in the small water population showed a tendency toward a coordinated gain in these signals. While we previously speculated that this increased accessibility might represent a poised or non-functional state, GO enrichment analysis of these specific regions revealed they are, in fact, functionally associated with adaptive responses. These regions were linked to nervous system development, such as synapse assembly (GO:0007416) and negative regulation of axon regeneration (GO:0048681), as well as the negative regulation of growth processes, including negative regulation of cell growth (GO:0030308) and negative regulation of developmental growth (GO:0048640) (Fig. S9).

2.5. Integrative multi-omics analysis and case study

Global correlation analysis confirmed that both chromatin accessibility and H3K27ac signals at promoters and enhancers are positively correlated with gene expression (Tables S12–S13). To identify high-confidence regulatory targets, we filtered for regions showing consistent directional changes across all three omics layers. We identified 7 enhancer regions where coordinated reductions in accessibility and H3K27ac signal were significantly associated with the downregulation of 5 target genes (Table S14). In contrast, no cases of coordinated

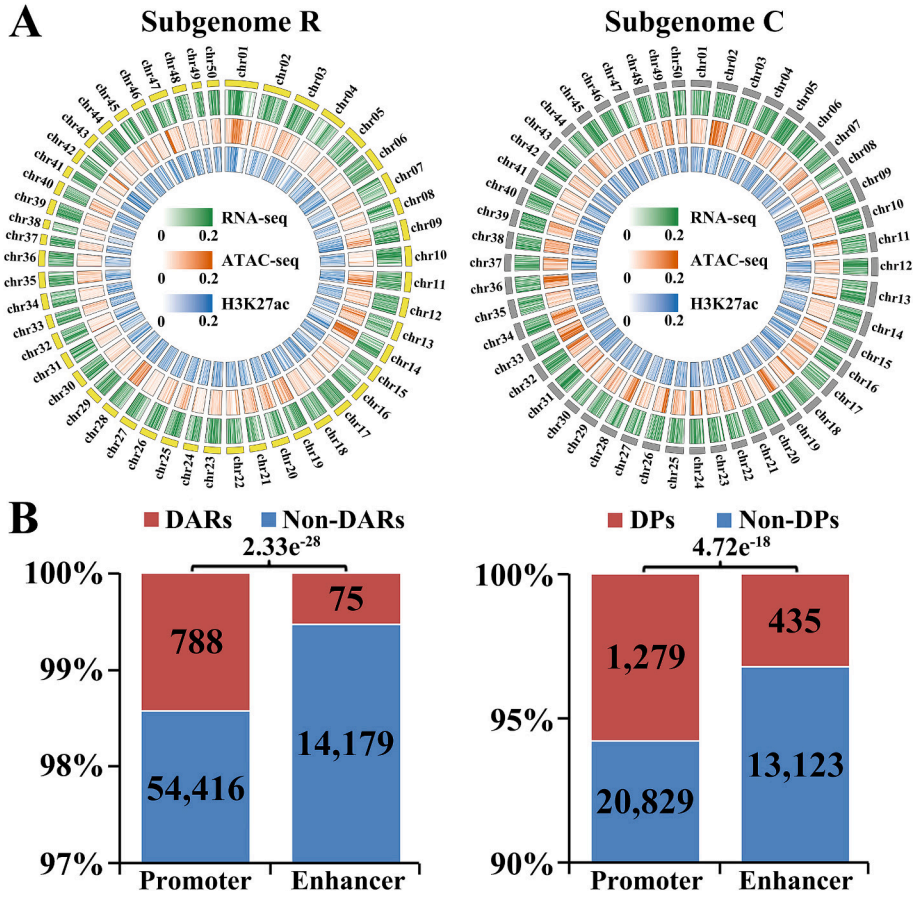


Fig. 4. Differential regulatory mechanisms of promoters and enhancers. (A) Circos plot showing the genomic distribution of differentially expressed genes (DEGs), differentially accessible regions (DARs), and differential H3K27ac peaks (DPs) across the chromosomes of the subgenomes R and C. (B) Comparison of the distribution of DARs and H3K27ac DPs between promoter and enhancer regions. The significance of the distributional difference was assessed using the Chi-square test ($p < 0.001$).

upregulation were detected. This indicates that coordinated repression of enhancer activity is a core mechanism restricting growth under spatial constraint.

The growth-related gene *rps6kb1a* serves as a prime example. In the small water population, *rps6kb1a* expression was significantly downregulated. Correspondingly, a key enhancer region located on the subgenome C (chr19: 10,137,810–10,138,014 bp) exhibited significant loss of both chromatin accessibility ($Log_2FC = -1.075$) and H3K27ac signal ($Log_2FC = -1.418$) (Fig. 5A–B). This provides direct evidence that environmental pressure limits somatic growth by remodeling the epigenetic state of specific enhancers associated with the mTOR pathway.

3. Discussion

The capacity to modulate somatic growth in response to ecological constraints is a fundamental adaptive strategy for indeterminate growers like fish. Large-scale biogeographical and phylogeographic analyses have unveiled a striking pattern: polyploid actinopterygians are disproportionately distributed in high-latitude or extreme environments compared to their diploid counterparts (David, 2022). This trend is particularly evident among East Asian cyprinids—including lineages of *Carassius*, *Schizothoracinae*, and *Sinocyclocheilus*—where polyploid species are predominantly concentrated in the fragmented, resource-limited inland water bodies of the Tibetan Plateau and adjacent regions, whereas diploid lineages dominate the lower reaches of major river systems and coastal areas (Liu et al., 2017; Li and Guo, 2020). These findings suggest that polyploidy confers a distinct adaptive advantage in coping with restricted environmental space (Li and Guo, 2020) However, while the phenotypic outcomes of such ecological confinement are well-documented, the molecular mechanisms translating spatial constraints into growth regulation remain elusive. In this study, by integrating multi-tissue transcriptomics, we demonstrate that water body size does not elicit a uniform systemic response but drives targeted transcriptional remodeling in the muscle (locomotion) and eye (sensory perception). Crucially, our epigenomic analysis reveals the mechanistic logic behind this adaptation: the restricted water environment forces a massive reduction in the total number of active genes through the extensive silencing of promoters, while simultaneously depressing the transcriptional amplitude of growth-related structural genes via the targeted inhibition of enhancers. Furthermore, we demonstrate that the two ancestral subgenomes contribute asymmetrically to this plasticity, providing a molecular basis for the ecological success of polyploid vertebrates.

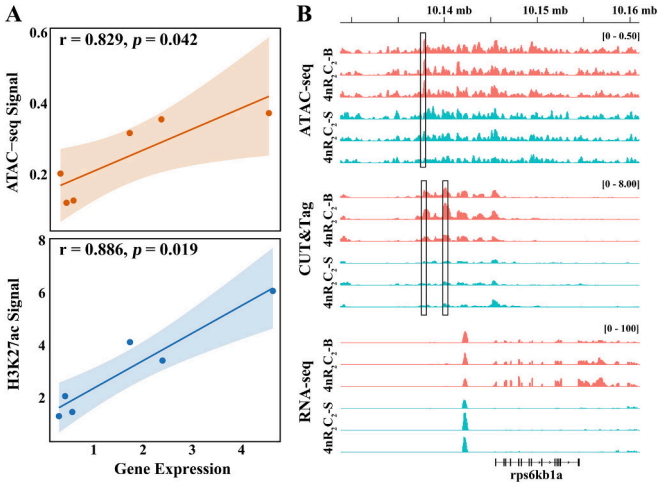


Fig. 5. Multi-omics validation of *rps6kb1a*. (A) Spearman correlation analysis between *rps6kb1a* mRNA expression levels and the epigenetic signals (chromatin accessibility and H3K27ac) at its associated enhancer region. (B) Integrative Genomics Viewer (IGV) tracks visualizing RNA-seq, ATAC-seq, and H3K27ac CUT&Tag signals at the *rps6kb1a* locus. The black square highlights the coordinated reduction of chromatin accessibility and histone modification at a specific enhancer region on the subgenome C in the small water population.

Our multi-tissue transcriptomic result reveals that the molecular response to spatial constraint is highly tissue-specific, rather than a uniform systemic adjustment. Among the eleven tissues examined, the eye and skeletal muscle exhibited the highest degree of transcriptional plasticity. The pronounced remodeling in skeletal muscle is consistent with its physiological role as the primary reservoir of somatic mass in teleosts (Wang et al., 2021; Ndandala et al., 2022; Yuan et al., 2024), a lineage characterized by indeterminate growth. In the restricted water environment, the widespread downregulation of structural genes associated with myofibril assembly and sarcomere organization provides a molecular explanation for the growth retardation phenotype. This suppression of myogenesis likely represents an adaptive bioenergetic strategy to limit somatic size in response to spatial confinement (Hudson, 2018; Sokolova, 2021). Meanwhile, the extensive transcriptional divergence observed in the eye suggests that visual perception serves as a primary sensory modality for detecting environmental spatial dimensions (Erikson et al., 2016; Caves et al., 2017). These transcriptomic patterns identify the eye and muscle as the primary responders to spatial constraints, where visual sensing is coupled with the targeted suppression of cytoskeletal assembly and mTOR signaling to physically limit somatic size.

Uncovering the epigenetic basis of this transcriptional remodeling, we identified a dual-layered regulatory strategy imposed by environmental constraints. The first layer involves the extensive silencing of promoter regions. Our data show that the loss of chromatin accessibility and histone acetylation at promoters in the small water population is directly coupled with a substantial reduction in the total number of expressed genes (from 47,553 to 39,256). This indicates that spatial restriction primarily acts by reducing the transcriptional breadth of the genome, effectively inactivating non-essential gene networks to conserve bioenergetic resources (Chiappino-Pepe et al., 2017; Vihervaara et al., 2017, 2018). The second layer involves the quantitative modulation of enhancers. Unlike the binary "on/off" pattern observed at promoters, enhancers associated with growth-related genes exhibited a coordinated reduction in signal intensity without complete silencing. This epigenetic dampening directly correlates with the decreased median expression levels of structural genes (e.g., cytoskeletal components), thereby limiting the transcriptional intensity of the somatic growth program. This specific decoupling of promoter and enhancer functions enables the organism to maintain basal cellular viability while physically constraining tissue hypertrophy, providing crucial insights into the molecular and genetic mechanisms underlying the spatial effect of water body size on individual development.

The adaptive potential of this allotetraploid lineage is underpinned by the asymmetric contribution of its ancestral subgenomes. We observed that the subgenome C consistently displays higher epigenetic plasticity and transcriptional heterogeneity compared to the subgenome R. This genomic asymmetry is functionally relevant, as evidenced by the regulation of *rps6kb1a*, a master regulator of the mTOR signaling pathway and protein synthesis. The suppression of *rps6kb1a* in the small water environment is driven by the targeted deactivation of a specific enhancer located on the subgenome C, rather than the subgenome R. This suggests a functional divergence where one subgenome (R) may preserve housekeeping stability, while the other (C) provides a dynamic regulatory repertoire to respond to environmental fluctuations (Xu et al., 2019; Luo et al., 2020). Such subgenome-specific plasticity likely confers an evolutionary advantage, enabling polyploid cyprinids to inhabit diverse and fragmented aquatic environments by modulating growth trajectories through a flexible portion of their genome without compromising core viability.

In conclusion, our study establishes a multi-dimensional regulatory framework linking ecological spatial constraints to somatic growth

adaptation. We demonstrate that water body size is not merely a physical boundary but a potent selective force that drives targeted transcriptional remodeling in sensory (eye) and locomotive (muscle) tissues. This adaptation is achieved through a distinct epigenetic mechanism: the reduction of the active gene pool via promoter silencing and the quantitative suppression of growth pathways via enhancer modulation. Moreover, this plasticity relies on the differential responsiveness of the ancestral subgenomes, highlighting the unique evolutionary advantage of polyploidy. These findings provide a comprehensive molecular explanation for how aquatic organisms epigenetically fine-tune their phenotypes to survive in spatially restricted habitats.

4. Materials and methods

4.1. Sample collection and experimental design

To investigate how different water body size environments epigenetically affect the growth phenotype of allopolyploid fish, we conducted the following study. We selected an allopolyploid lineage population ($4nR_2C_2$) which was obtained by intergeneric hybridization between goldfish (*Carassius auratus*) and common carp (*Cyprinus carpio*), Both pools (small: 8.8 m × 4.7 m × 1.4 m; large: 50.0 m × 65.0 m × 2.5 m) maintained similar environmental conditions, including illumination, water temperature, adequate food supply, and appropriate oxygen content. One thousand $4nR_2C_2$ fry were randomly stocked into each of two ponds (one small, one large) in May 2020. These fish (F_1) became sexually mature at one year (Liu et al., 2001). Following the breeding season, adult fish were removed from both pools, and the resulting fry (F_2) were raised until April 2022. A random sample of 3 healthy 12-month-old juvenile fish was collected from each pool in April 2022. Gonadal examination of the samples revealed a sex distribution of 2 males and 4 females. These fish were deeply anesthetized with 300 mg/L Tricaine Methanesulfonate (Sigma-Aldrich, St. Louis, MO, USA) for 10 min (25 °C) in a separate tank. After euthanasia, the fish were immediately dissected, and 11 tissues (intestine, spleen, liver, heart, kidney, pituitary, brain, eye, ovary, testis, and muscle) were collected immediately.

4.2. RNA isolation and mRNA-seq data analysis

Total RNA was isolated from 11 tissues (intestine, spleen, liver, heart, kidney, pituitary, brain, eye, ovary, testis, muscle) and purified according to a TRIzol extraction method (Rio et al., 2010). RNA concentration was measured using NanoDrop technology. Total RNA samples were treated with DNase I (Invitrogen) to remove any contaminating genomic DNA. The purified RNA was quantified using a 2100 Bioanalyzer system (Agilent, Santa Clara, CA, USA). 1 μg of isolated mRNA was fragmented with fragmentation buffer. Paired-end (2 × 150 bp) sequencing was performed using DNBSEQ-T7 platform according to the standard method (Patterson et al., 2019). Then, low-quality bases and adapters were trimmed out by Fastp (v. 0.21.0) (Chen et al., 2018). All mRNA sequencing reads were aligned to the nuclear and mitochondrial genomes of goldfish and common carp using BWA-MEM (v.0.7.17) (Li and Durbin, 2010) with default parameters. The mapped files were processed using Samtools (v.1.10) (Li et al., 2009), and uniquely mapped reads were counted using htseq-count (Srinivasan et al., 2020). Raw read counts generated by htseq-count were used for differential expression analysis with DESeq2 (v1.32.0) (Love et al., 2014), with genes considered significantly differentially expressed if $|\log_2\text{FoldChange}| > 1$ and the adjusted padj <0.05. Gene expression levels were normalized based on the proportion of reads mapped to each gene relative to the total mapped reads across the genome and expressed as transcripts per million (TPM). In addition, to visualize gene expression patterns across multiple tissues, the gene expression matrix of all samples was subjected to clustering analysis and principal component analysis to assess tissue-specific expression and differences between populations.

4.3. ATAC-seq data generation and processing

Muscle tissues used for ATAC-seq were obtained from the same six samples described above for RNA-seq. The samples were first washed with 0.09% NaCl solution and then ground into powder in liquid nitrogen. The powders were treated with lysis buffer and incubated for 10 min at 4 °C on a rotation mixer. The resulting cell suspension was filtered through a 40 μm cell strainer and washed three times with cold PBS buffer. After inspecting nuclei purity and intactness under microscopy, approximately 50,000 nuclei were allocated to perform tagmentation according to standard protocols (Corces et al., 2017) and Tn5 transposed DNA was purified by AMPure DNA magnetic beads. A qPCR reaction was performed on a subset of the DNA to determine the optimum number (average 11) of PCR cycles, and amplified libraries were run on an Agilent Tapestation 2200 using a D5000 DNA ScreenTape to assess quality by visualizing nucleosomal laddering. Replicates were performed in duplicate for all ATAC experiments. The final library was sequenced on the Illumina HiSeq X Ten platform (San Diego, CA, United States) with paired-end 150 bp.

Prior to mapping, standard next-generation sequencing quality control steps using cutadapt (http://cutadapt.readthedocs.io/en/stable) (1.9.1), as well as ATAC-seq-specific quality control steps, were performed. Trimmed reads were aligned to reference genomes using Bowtie2 (version 2.2.6) (Langmead and Salzberg, 2012), and reads mapping to the mitochondrial genome were removed using removeChrom (https://github.com/jsh58/harvard). PCR duplicates were removed and the number of mapped reads downsampled to a standard of approximately 20 M using Picard (version 1.126) (http://broadinstitute.github.io/picard/) for the samples. Peaks were called for each biological replicate using MACS2 (Zhang et al., 2008). Peaks identified in all three biological replicates were considered to have high-to-medium confidence. We performed IDR assessment on peaks between each sample and self-pseudoreplicates with IDR threshold set to 0.05. All peaks from all samples were merged to generate a consensus peak set. For each consensus peak, its enrichment was defined as ATAC signal intensity (normalized read count per base) subtracted by the background noise (normalized read count per base). The R package DESeq2 (v1.32.0) (Love et al., 2014) was used to identify potential differentially accessible regions (DARs) from the consensus peak set. Statistically significant DARs were defined as peaks with $|\log_2\text{FoldChange}| > 1$ and p-value <0.05. Motif analysis on DARs was performed using MEME (Heinz et al., 2010) suite with default settings, and only motifs with P value <0.01 were retained. Gene ontology enrichment analysis was conducted using the R package ClusterProfiler (v4.0.0) (Wu et al., 2021) with default parameters. All sequencing tracks were visualized using the Integrated Genomic Viewer (IGV, v2.3.61) (Thorvaldsdóttir et al., 2013).

4.4. CUT&Tag data generation and processing

CUT&Tag experiments targeting H3K27ac were performed on muscle tissues from the same six individuals used for ATAC-seq and RNA-seq. Approximately 100,000 cells were obtained from the six muscle samples were centrifuged for 3 min at 600 ×g at room temperature (Kaya-Okur et al., 2019). Cells were washed twice in 300 μL Wash Buffer (20 mM HEPES, pH 7.5; 150 mM NaCl; 0.5 mM Spermidine; 1× Protease inhibitor cocktail) by gentle pipetting. Each sample was then incubated with 10 μL of activated concanavalin A-coated magnetic beads at room temperature for 10 min. After removing the unbound supernatant, and bead-bound cells were resuspended in 50 μL Dig-wash Buffer (20 mM HEPES, pH 7.5; 150 mM NaCl; 0.5 mM Spermidine; 1× Protease inhibitor cocktail; 0.05% Digitonin) containing 2 mM EDTA and a 1:50 dilution of the appropriate primary antibody. Primary antibody incubation was performed on a rotating platform for 2 h at room temperature. The liquid was then removed using a magnetic stand. An

appropriate secondary antibody was diluted 1:50 in 50 μL Dig-wash buffer, and cells were incubated at room temperature for 1 h. For the negative control library (IgG only), no primary antibody was added. Cells were washed twice for 1 min in 500 μL Dig-wash buffer on the magnetic stand to remove unbound antibodies. A 1:200 dilution of pG-Tn5 adapter complex (approximately 0.04 μM) was prepared in Dig-300 Buffer (0.01% Digitonin, 20 mM HEPES, pH 7.5, 300 mM NaCl, 0.5 mM Spermidine, 1× Protease inhibitor cocktail). After removing the liquid, 100 μL was added to the cells with gentle vortexing and incubated with pG-Tn5 at room temperature for 1 h. Cells were washed twice for 1 min in 500 μL Dig-300 Buffer to remove unbound pG-Tn5 protein. Cells were then resuspended in 300 μL Tagmentation buffer (10 mM $MgCl_2$ in Dig-300 Buffer) and incubated at 37 °C for 1 h. To stop tagmentation, 10 μL of 0.5 M EDTA, 3 μL of 10% SDS, and 2.5 μL of 20 mg/mL Proteinase K were added to 300 μL of sample, incubated at 55 °C for 1 h, purified using phenol–chloroform–isoamyl alcohol and ethanol, washed with 100% ethanol, and suspended in water. The DNA was amplified by PCR as follows: 3 min at 72 °C and 30s at 98 °C, followed by 16 cycles of 15 s at 98 °C, 30 s at 60 °C, and 30s at 72 °C, with a final extension at 72 °C for 3 min. Finally, the amplified DNA was purified using Ampure XP beads. Libraries were sequenced on the Illumina Nova-seq platform.

FastQC (v0.11.9) (https://www.bioinformatics.babraham.ac.uk/projects/fastqc/) with default parameters was used to assess read quality. Adapter trimming and quality filtering were performed using Trimmomatic (v0.39) (Bolger et al., 2014) to remove adapters, low-quality bases, and reads shorter than 8 nt. Clean reads were aligned to the merged genomes of goldfish and common carp using Bowtie2 (v2.2.6) (Langmead and Salzberg, 2012) with the options -X 1000 –very-sensitive. PCR duplicates were removed using Picard MarkDuplicates. Peak calling was performed using MACS2 (Zhang et al., 2008), and peaks were filtered using a q-value threshold <0.05. Peak calls from each replicate across both controls and treatments were merged into a union set using bedtools merge. Differential peaks were identified using DESeq2 (v1.32.0) (Love et al., 2014) with default parameters; regions with p-value <0.05 and $|\log_2\text{FoldChange}| > 1$ were considered statistically significant. Heatmaps were generated using ComplexHeatmap. Peaks were annotated to the nearest feature using ChIPseeker (v1.32.0) (Yu et al., 2015). GO and KEGG enrichment analysis was performed using ClusterProfiler (v4.0.0) (Wu et al., 2021). Consensus motif sequence analysis was conducted using HOMER. Normalized CUT&Tag signals were derived from bigwig files using bedGraphToBigWig and visualized in Integrative Genomics Viewer (v2.8.0) (Thorvaldsdóttir et al., 2013).

4.5. Enhancer identification

Open chromatin regions obtained from ATAC-seq were first overlapped with H3K27ac histone modification signals using bedtools (v2.31.1) (Quinlan and BEDTools, 2010) with default settings. To avoid promoter interference, regions located within ±2 kb of transcription start sites (TSS) were excluded. The remaining overlapping regions were initially defined as candidate enhancer regions. These regions were then processed separately for the $4nR_2C_2$-S and $4nR_2C_2$-B sample groups, retaining only regions that were present in at least three samples within each group to improve confidence in enhancer identification. Genomic annotation of candidate enhancers was performed using ChIPseeker (v1.32.1) (Yu et al., 2015).

4.6. Correlation analysis between gene expression and epigenetic features

Spearman correlation coefficients were calculated between gene expression and chromatin accessibility (ATAC-seq), as well as between gene expression and H3K27ac signal intensity. Spearman correlation analysis was performed in Python using the spearmanr function from the scipy.stats package. To define enhancer-promoter pairs, we linked each gene's promoter (TSS ± 2 kb) to all potential enhancers located within a ± 100 kb window of the transcription start site (TSS). This distance-based pairing was executed using bedtools (v2.31.1) (Quinlan and BEDTools, 2010). Enhancer–gene assignment was performed using a Spearman correlation based approach. Putative target genes were defined as genes located within ±100 kb of each enhancer. For each enhancer–gene pair, Spearman correlations were calculated between gene expression and enhancer accessibility, and between gene expression and H3K27ac enrichment. Enhancer–gene links were considered significant only when gene expression showed significant correlations ($r > 0$ and $p < 0.05$) with both ATAC-seq signal and H3K27ac. Permutation testing (5000 iterations) demonstrated that the mean correlation of the specified enhancer-gene pairs significantly exceeded that of randomly shuffled pairs ($p < 0.001$).

Key genes were selected if they simultaneously met the following criteria: the gene was significantly differentially expressed between populations; the promoter or enhancer regions showed significantly altered chromatin accessibility or H3K27ac enrichment between the two groups; and the gene expression was positively correlated with the epigenetic signal (Spearman $r > 0$, $p < 0.05$). For selected key candidate genes, genome browser tracks (ATAC-seq, H3K27ac, and RNA-seq) were visualized using Integrative Genomics Viewer (Thorvaldsdóttir et al., 2013) to illustrate the relationship between gene expression and the epigenetic state of the promoter and putative enhancer regions.

CRediT authorship contribution statement

Yiyan Zeng: Writing – original draft, Formal analysis, Conceptualization. **Jinhui Zhang:** Investigation. **Qingxi Wang:** Investigation. **Xiaohuan Han:** Investigation. **Ling Liu:** Investigation. **Kai Yang:** Investigation. **Ruyi Zhang:** Investigation. **Kaikun Luo:** Investigation. **Li Ren:** Writing – review & editing, Writing – original draft, Supervision, Funding acquisition, Conceptualization. **Shaojun Liu:** Supervision, Funding acquisition.

Consent for publication

Not applicable.

Ethics approval and consent to participate

All experimental procedures involving animals were reviewed and approved by the Academic Committee of Hunan Normal University, Hunan, China (Approval number: 2022R003).

Funding

This research was supported by National Natural Science Foundation of China (32341057 and 32293252), National Key Research and Development Program of China (2023YFD2401602), Special Funds for Construction of Innovative Provinces in Hunan Province (2021NK1010), Earmarked Fund for China Agriculture Research System (CARS-45), and 111 Project (D20007), and The world-class cultivation discipline (Biology) of Hunan province.

Declaration of competing interest

The authors declare no competing interests.

Acknowledgements

Not applicable.

Appendix A. Supplementary data

Supplementary data to this article can be found online at https://doi.

org/10.1016/j.cbd.2026.101787.

Data availability

Data will be made available on request.

References

Abdelnour, S.A., Naiel, M.A., Said, M.B., Alnajeebi, A.M., Nasr, F.A., Al-Doaiss, A.A., Mahasneh, Z.M., Noreldin, A.E., 2024. Environmental epigenetics: exploring phenotypic plasticity and transgenerational adaptation in fish. Environ. Res. 252, 118799. https://doi.org/10.1016/j.envres.2024.118799.

Ahti, P.A., Kuparinen, A., Uusi-Heikkilä, S., 2020. Size does matter—the eco-evolutionary effects of changing body size in fish. Environ. Rev. 28 (3), 311–324. https://doi.org/10.1139/er-2019-0076.

Audzijonyte, A., Richards, S.A., Stuart-Smith, R.D., Pecl, G., Edgar, G.J., Barrett, N.S., Payne, N., Blanchard, J.L., 2020. Fish body sizes change with temperature but not all species shrink with warming. Nat. Ecol. Evol. 4 (6), 809–814. https://doi.org/10.1038/s41559-020-1171-0.

Bolger, A.M., Lohse, M., Usadel, B., 2014. Trimmomatic: a flexible trimmer for Illumina sequence data. Bioinformatics 30 (15), 2114–2120. https://doi.org/10.1093/bioinformatics/btu170.

Caves, E.M., Sutton, T.T., Johnsen, S., 2017. Visual acuity in ray-finned fishes correlates with eye size and habitat. J. Exp. Biol. 220 (9), 1586–1596. https://doi.org/10.1242/jeb.151183.

Chen, S., Zhou, Y., Chen, Y., Gu, J., 2018. fastp: an ultra-fast all-in-one FASTQ preprocessor. Bioinformatics 34, i884–i890. https://doi.org/10.1093/bioinformatics/bty560.

Chen, D., Zhang, Q., Tang, W., Huang, Z., Wang, G., Wang, Y., Shi, J., Xu, H., Lin, L., Li, Z., Chi, W., Huang, L., Xia, J., Zhang, X., Guo, L., Wang, Y., Ma, P., Tang, J., Zhou, G., Liu, M., Liu, F., Hua, X., Wang, B., Shen, Q., Jiang, Q., Lin, J., Chen, X., Wang, H., Dou, M., Liu, L., Pan, H., Qi, Y., Wu, B., Fang, J., Zhou, Y., Cen, W., He, W., Zhang, Q., Xue, T., Lin, G., Zhang, W., Liu, Z., Qu, L., Wang, A., Ye, Q., Chen, J., Zhang, Y., Ming, R., Van Montagu, M., Tang, H., Van de Peer, Y., Chen, Y., Zhang, J., 2020. The evolutionary origin and domestication history of goldfish (*Carassius auratus*). Proc. Natl. Acad. Sci. USA 117 (47), 29775–29785. https://doi.org/10.1073/pnas.2005545117.

Chiappino-Pepe, A., Tymoshenko, S., Ataman, M., Soldati-Favre, D., Hatzimanikatis, V., 2017. Bioenergetics-based modeling of *Plasmodium falciparum* metabolism reveals its essential genes, nutritional requirements, and thermodynamic bottlenecks. PLoS Comput. Biol. 13 (3), e1005397. https://doi.org/10.1371/journal.pcbi.1005397.

Corces, M.R., Trevino, A.E., Hamilton, E.G., Greenside, P.G., Sinnott-Armstrong, N.A., Vesuna, S., Satpathy, A.T., Rubin, A.J., Montine, K.S., Wu, B., 2017. An improved ATAC-seq protocol reduces background and enables interrogation of frozen tissues. Nat. Methods 14 (10), 959–962. https://doi.org/10.1038/nmeth.4396.

David, K.T., 2022. Global gradients in the distribution of animal polyploids. Proc. Natl. Acad. Sci. 119 (48), e2214070119. https://doi.org/10.1073/pnas.2214070119.

Erikson, U., Gansel, L., Frank, K., Svendsen, E., Digre, H., 2016. Crowding of Atlantic salmon in net-pen before slaughter. Aquaculture 465, 395–400. https://doi.org/10.1016/j.aquaculture.2016.09.018.

Heinz, S., Benner, C., Spann, N., Bertolino, E., Lin, Y.C., Laslo, P., Cheng, J.X., Murre, C., Singh, H., Glass, C.K., 2010. Simple combinations of lineage-determining transcription factors prime cis-regulatory elements required for macrophage and B cell identities. Mol. Cell 38 (4), 576–589. https://doi.org/10.1016/j.molcel.2010.05.004.

Hudson, R., 2018. Body size, energetics, and adaptive radiation. In: Bioenergetics of Wild Herbivores. CRC Press.

Kaya-Okur, H.S., Wu, S.J., Codomo, C.A., Pledger, E.S., Bryson, T.D., Henikoff, J.G., Ahmad, K., Henikoff, S., 2019. CUT&Tag for efficient epigenomic profiling of small samples and single cells. Nat. Commun. 10 (1), 1930. https://doi.org/10.1038/s41467-019-09982-5.

Langmead, B., Salzberg, S.L., 2012. Fast gapped-read alignment with Bowtie 2. Nat. Methods 9 (4), 357–359. https://doi.org/10.1038/nmeth.1923.

Li, H., Durbin, R., 2010. Fast and accurate long-read alignment with Burrows–Wheeler transform. Bioinformatics 26 (5), 589–595. https://doi.org/10.1093/bioinformatics/btp698.

Li, X., Guo, B., 2020. Substantially adaptive potential in polyploid cyprinid fishes: evidence from biogeographic, phylogenetic and genomic studies. Proc. R. Soc. B 287 (1920), 20193008. https://doi.org/10.1098/rspb.2019.3008.

Li, H., Handsaker, B., Wysoker, A., Fennell, T., Ruan, J., Homer, N., Marth, G., Abecasis, G., Durbin, R., Subgroup, G. P. D. P, 2009. The sequence alignment/map format and SAMtools. Bioinformatics 25 (16), 2078–2079. https://doi.org/10.1093/bioinformatics/btp352.

Liu, S., Liu, Y., Zhou, G., Zhang, X., Luo, C., Feng, H., He, X., Zhu, G., Yang, H., 2001. The formation of tetraploid stocks of red crucian carp x common carp hybrids as an effect of interspecific hybridization. Aquaculture 192 (2–4), 171–186. https://doi.org/10.1016/S0044-8486(00)00451-8.

Liu, S., Luo, J., Chai, J., Ren, L., Zhou, Y., Huang, F., Liu, X., Chen, Y., Zhang, C., Tao, M., Lu, B., Zhou, W., Lin, G., Mai, C., Yuan, S., Wang, J., Li, T., Qin, Q., Feng, H., Luo, K., Xiao, J., Zhong, H., Zhao, R., Duan, W., Song, Z., Wang, Y., Wang, J., Zhong, L., Wang, L., Ding, Z., Du, Z., Lu, X., Gao, Y., Murphy, R.W., Liu, Y., Meyer, A., Zhang, Y. P., 2016. Genomic incompatibilities in the diploid and tetraploid offspring of the goldfish x common carp cross. Proc. Natl. Acad. Sci. USA 113 (5), 1327–1332. https://doi.org/10.1073/pnas.1512955113.

Liu, X.-L., Jiang, F.-F., Wang, Z.-W., Li, X.-Y., Li, Z., Zhang, X.-J., Chen, F., Mao, J.-F., Zhou, L., Gui, J.-F., 2017. Wider geographic distribution and higher diversity of hexaploids than tetraploids in *Carassius* species complex reveal recurrent polyploidy effects on adaptive evolution. Sci. Rep. 7 (1), 5395. https://doi.org/10.1038/s41598-017-05731-0.

Love, M.I., Huber, W., Anders, S., 2014. Moderated estimation of fold change and dispersion for RNA-seq data with DESeq2. Genome Biol. 15 (12), 550. https://doi.org/10.1186/s13059-014-0550-8.

Luo, J., Chai, J., Wen, Y., Tao, M., Lin, G., Liu, X., Ren, L., Chen, Z., Wu, S., Li, S., Wang, Y., Qin, Q., Wang, S., Gao, Y., Huang, F., Wang, L., Ai, C., Wang, X., Li, L., Ye, C., Yang, H., Luo, M., Chen, J., Hu, H., Yuan, L., Zhong, L., Wang, J., Xu, J., Du, Z., Ma, Z., Murphy, R.W., Meyer, A., Gui, J., Xu, P., Ruan, J., Chen, Z.J., Liu, S., Lu, X., Zhang, Y.-p., 2020. From asymmetrical to balanced genomic diversification during rediploidization: subgenomic evolution in allotetraploid fish. Sci. Adv. 6 (22), eaaz7677. https://doi.org/10.1126/sciadv.aaz7677.

Ndandala, C.B., Dai, M., Mustapha, U.F., Li, X., Liu, J., Huang, H., Li, G., Chen, H., 2022. Current research and future perspectives of GH and IGFs family genes in somatic growth and reproduction of teleost fish. Aquacult. Rep. 26, 101289. https://doi.org/10.1016/j.aqrep.2022.101289.

Oke, K.B., Cunningham, C., Westley, P., Baskett, M., Carlson, S., Clark, J., Hendry, A., Karatayev, V., Kendall, N., Kibele, J., 2020. Recent declines in salmon body size impact ecosystems and fisheries. Nat. Commun. 11 (1), 4155. https://doi.org/10.1038/s41467-020-17726-z.

Parsons, K.J., Robinson, B.W., 2006. Replicated evolution of integrated plastic responses during early adaptive divergence. Evolution 60 (4), 801–813. https://doi.org/10.1111/j.0014-3820.2006.tb01158.x.

Patterson, J., Carpenter, E.J., Zhu, Z., An, D., Liang, X., Geng, C., Drmanac, R., Wong, G. K.-S., 2019. Impact of sequencing depth and technology on de novo RNA-Seq assembly. BMC Genomics 20 (1), 604. https://doi.org/10.1186/s12864-019-5965-x.

Quinlan, A., BEDTools, I. H, 2010. A flexible suite of utilities for comparing genomic features, 26, 841–842. https://doi.org/10.1093/bioinformatics/btq033.

Ren, L., Gao, X., Cui, J., Zhang, C., Dai, H., Luo, M., He, S., Qin, Q., Luo, K., Tao, M., Xiao, J., Wang, J., Zhang, H., Zhang, X., Zhou, Y., Wang, J., Zhao, X., Liu, G., Wang, G., Huo, L., Wang, S., Hu, F., Zhao, R., Zhou, R., Wang, Y., Liu, Q., Yan, X., Wu, C., Yang, C., Tang, C., Duan, W., Liu, S., 2022. Symmetric subgenomes and balanced homoeolog expression stabilize the establishment of allopolyploidy in cyprinid fish. BMC Biol. 20 (1). https://doi.org/10.1186/s12915-022-01401-4.

Rio, D.C., Ares, M., Hannon, G.J., Nilsen, T.W., 2010. Purification of RNA using TRIzol (TRI reagent). Cold Spring Harb Protoc 2010 (6), pdb.prot5439. https://doi.org/10.1101/pdb.prot5439.

Sokolova, I., 2021. Bioenergetics in environmental adaptation and stress tolerance of aquatic ectotherms: linking physiology and ecology in a multi-stressor landscape. J. Exp. Biol. 224 (Suppl_1), jeb236802. https://doi.org/10.1242/jeb.236802.

Srinivasan, K.A., Virdee, S.K., McArthur, A.G., 2020. Strandedness during cDNA synthesis, the stranded parameter in htseq-count and analysis of RNA-Seq data. Brief. Funct. Genomics 19 (5–6), 339–342. https://doi.org/10.1093/bfgp/elaa010.

Thorson, J.L., Smithson, M., Beck, D., Sadler-Riggleman, I., Nilsson, E., Dybdahl, M., Skinner, M.K., 2017. Epigenetics and adaptive phenotypic variation between habitats in an asexual snail. Sci. Rep. 7 (1), 14139. https://doi.org/10.1038/s41598-017-14673-6.

Thorvaldsdóttir, H., Robinson, J.T., Mesirov, J.P., 2013. Integrative Genomics Viewer (IGV): high-performance genomics data visualization and exploration. Brief. Bioinform. 14 (2), 178–192. https://doi.org/10.1093/bib/bbs017.

Van de Peer, Y., Mizrachi, E., Marchal, K., 2017. The evolutionary significance of polyploidy. Nat. Rev. Genet. 18 (7), 411–424. https://doi.org/10.1038/nrg.2017.26.

Van de Peer, Y., Ashman, T.-L., Soltis, P.S., Soltis, D.E., 2021. Polyploidy: an evolutionary and ecological force in stressful times. Plant Cell 33 (1), 11–26. https://doi.org/10.1093/plcell/koab149.

Vihervaara, A., Mahat, D.B., Guertin, M.J., Chu, T., Danko, C.G., Lis, J.T., Sistonen, L., 2017. Transcriptional response to stress is pre-wired by promoter and enhancer architecture. Nat. Commun. 8 (1), 255. https://doi.org/10.1038/s41467-017-00151-0.

Vihervaara, A., Duarte, F.M., Lis, J.T., 2018. Molecular mechanisms driving transcriptional stress responses. Nat. Rev. Genet. 19 (6), 385–397. https://doi.org/10.1038/s41576-018-0001-6.

Wang, Y., Hong, D., Yao, J., Tan, H., Wang, S., Li, J., Luo, Y., Wang, D., Liu, S., 2021. Comparative transcriptome preliminary reveals the molecular mechanism of the growth rate of *Procambarus clarkii*. Reprod. Breed. 1 (4), 204–209. https://doi.org/10.1016/j.repbre.2021.11.003.

Woolnough, D., Downing, J., Newton, T., 2009. Fish movement and habitat use depends on water body size and shape. Ecol. Freshw. Fish 18 (1), 83–91. https://doi.org/10.1111/j.1600-0633.2008.00326.x.

Wu, T., Hu, E., Xu, S., Chen, M., Guo, P., Dai, Z., Feng, T., Zhou, L., Tang, W., Zhan, L., 2021. ClusterProfiler 4.0: a universal enrichment tool for interpreting omics data. Innovation 2 (3). https://doi.org/10.1016/j.xinn.2021.100141.

Xu, P., Zhang, X., Wang, X., Li, J., Liu, G., Kuang, Y., Xu, J., Zheng, X., Ren, L., Wang, G., Zhang, Y., Huo, L., Zhao, Z., Cao, D., Lu, C., Li, C., Zhou, Y., Liu, Z., Fan, Z., Shan, G., Li, X., Wu, S., Song, L., Hou, G., Jiang, Y., Jeney, Z., Yu, D., Wang, L., Shao, C., Song, L., Sun, J., Ji, P., Wang, J., Li, Q., Xu, L., Sun, F., Feng, J., Wang, C., Wang, S., Wang, B., Li, Y., Zhu, Y., Xue, W., Zhao, L., Wang, J., Gu, Y., Lv, W., Wu, K., Xiao, J., Wu, J., Zhang, Z., Yu, J., Sun, X., 2014. Genome sequence and genetic diversity of the common carp, *Cyprinus carpio*. Nat. Genet. https://doi.org/10.1038/ng.3098.

Xu, P., Xu, J., Liu, G.J., Chen, L., Zhou, Z.X., Peng, W.Z., Jiang, Y.L., Zhao, Z.X., Jia, Z.Y., Sun, Y.H., Wu, Y.D., Chen, B.H., Pu, F., Feng, J.X., Luo, J., Chai, J., Zhang, H.Y., Wang, H., Dong, C.J., Jiang, W.K., Sun, X.W., 2019. The allotetraploid origin and

asymmetrical genome evolution of the common carp *Cyprinus carpio*. Nat. Commun. 10 (1), 4625. https://doi.org/10.1038/s41467-019-12644-1.

Yu, G., Wang, L.-G., He, Q.-Y., 2015. ChIPseeker: an R/Bioconductor package for ChIP peak annotation, comparison and visualization. Bioinformatics 31 (14), 2382–2383. https://doi.org/10.1093/bioinformatics/btv145.

Yuan, X., Tao, L., Hu, X., Lin, R., Yang, J., Feng, M., Peng, M., Liu, W., Xiao, Y., 2024. Expression profile analysis of muscle regulation genes under growth and water flow stress in zebrafish. Reprod. Breed. 4 (1), 5–9. https://doi.org/10.1016/j.repbre.2023.12.004.

Zhang, Y., Liu, T., Meyer, C.A., Eeckhoute, J., Johnson, D.S., Bernstein, B.E., Nusbaum, C., Myers, R.M., Brown, M., Li, W., 2008. Model-based analysis of ChIP-Seq (MACS). Genome Biol. 9 (9), R137. https://doi.org/10.1186/gb-2008-9-9-r137.